



Characterization, thermal degradation kinetics, and morphological properties of a graphene oxide/poly (vinyl alcohol)/starch nanocomposite

Esmat Sedaghat¹ · Abbas Ali Rostami¹ · Mousa Ghaemy¹ · Ali Rostami²

Received: 2 April 2018 / Accepted: 12 August 2018 / Published online: 24 August 2018
© Akadémiai Kiadó, Budapest, Hungary 2018

Abstract

In this study, we synthesized a biodegradable nanocomposite containing starch, polyvinyl alcohol (PVA), and graphene oxide (GO). The non-isothermal degradation kinetics of this nanocomposite was investigated by thermogravimetric analysis. Accordingly, the kinetic parameters, such as activation energy (E_a), exponential factor (A), rate constant (k), and degradation time, were calculated. The calculated kinetic parameters are used to predict the lifetime. The master plot analysis showed that the kinetic function of the thermal degradation changed from A_2 to A_3 upon addition of GO to the PVA/starch blend. The reaction heat (ΔH), glass transition temperature (T_g), and melting point (T_m) of the PVA/starch film and PVA/starch/GO nanocomposite were determined by the differential scanning calorimetry analysis. Also, the T_g values were determined by dynamic mechanical thermal analyzer. The changes in peak bandwidth, strength, and frequency in the samples are identified by FTIR spectra. The structure and morphology of the nanocomposite were studied by X-ray diffraction analysis and field emission scanning electronic microscope.

Keywords Thermal degradation · Master plots · PVA/starch/graphene oxide · Nanocomposite

Introduction

The study on the thermal degradation of biodegradable polymers is of great importance because of their various applications such as coatings, electrical insulators, adhesives, matrices in reinforced composites [1]. Knowing the behavior of high-performance biodegradable nanocomposites at high temperatures is crucial. Therefore, it is necessary to study the thermal degradation of biodegradable composites to have an insight into the mechanism and lifetime of the process. One of the most famous biodegradable polymers is starch consisting of two types of carbohydrate polymers known as amylose and amylopectin [2, 3]. Some properties of starch including gelation, water

solubility, and surface properties depend on the amylose and amylopectin composition [4–9]. The advantages of starch, such as abundance in nature, biocompatibility, biodegradability, easy functionalization, and relatively easy isolation from their natural sources, have led to their extensive applications, especially in the field of biomaterials and drug delivery [6, 10–15]. Unlike unique characteristics of starch, its poor mechanical properties limit its applications. Hence, some researchers have tried to overcome the drawbacks by combining starch with other compounds such as biodegradable synthetic polymers [16–18]. For instance, PVA has been widely used as one of these compounds due to its biocompatibility, non-toxicity, water solubility, and good chemical and thermal stability. PVA has a large number of hydroxyl groups, which provides a biocompatible microenvironment. PVA/thermoplastic starch blends have many beneficial properties and can be used in a broad range of applications [19–21]. To further improve the characteristics of such blends, some physical and chemical methods, such as cross-linking and incorporation of nanofillers, can be applied [22]. Nanofillers, such as graphene oxide, are known to improve the

✉ Esmat Sedaghat
eamatsedaghat779@gmail.com

¹ Faculty of Chemistry, University of Mazandaran,
P. O. Box 453, Babolsar, Iran

² Faculty of Science, University of Nizwa, Birkat Al Mawz,
Oman

mechanical, thermal, and electrical properties of polymer. GO with excellent thermal, mechanical, and a barrier property is one of the popular nanomaterials obtained from graphite. It is frequently used for the preparation of polymer/GO hybrid nanocomposites with improved properties [23, 24]. The hydrophilic characteristic of GO, arisen from various oxygen-containing functional groups including hydroxyl, epoxide, carbonyl, and carboxyl, leads to the formation of strong physical bonds between GO and hydrophilic polymers such as starch and gelatin. In other words, compatibility between GO and the mentioned polymers makes them more miscible, which is necessary to produce the polymer/GO hybrid nanocomposites [25–27]. The high electrical conductivity of GO is due to its free electrons.

TGA has been widely used by many authors to investigate the thermal degradation kinetics of nanocomposites. For instance, Susmita et al. studied the thermal stability of PVA/starch films by using organically modified MMTs. They showed that addition of starch to the PVA matrix reduced the thermal stability of PVA, while addition of nanoclay at 1, 2, and 3% loading resulted in the improvement of stability [28]. Amalia et al. studied the physical and microstructural properties of PVA/starch and showed that the incorporation of PVA into pea starch films improved their physical properties [17]. Bhanu Priya et al. investigated the synthesis, characterization, and antibacterial activity of biodegradable starch/PVA composite films reinforced with cellulosic fiber and found that the mechanical properties of fiber-reinforced starch/PVA composite blend films were higher than those of the starch/PVA cross-linked blend films containing 20% of *G. optiva* fiber [15]. Taghizadeh et al. studied the thermal degradation of starch/PVA blend [8].

The aim of the present work is to investigate the effect of GO on the thermophysical, morphological, and electrical properties of the PVA/starch/GO nanocomposites. Also, the degradation kinetics of the nanocomposite was studied to have an insight on the involved degradation mechanism. The prepared nanocomposites were characterized using TGA, DSC, DMTA, FESEM, and XRD.

Materials

GO, dispersed in H₂O (2 mg mL⁻¹), was kindly supplied by Aldrich Chemical Co. The used extra pure starch, soluble in water (0.02 g mL⁻¹, 25 °C) with the molecular weight of 342.30 g mol⁻¹, pH = 6.0–7.5 and the bulk density of 0.3 g cm⁻³, was purchased from Merck Co. PVA 49,000 ($M_w = 49,000$, degree of hydrolysis 86–89 mol%) was purchased from Fluka, Switzerland. Glycerol ($M_n = 92.10$, grade of pure 85%), as starch

plasticizer, was provided by Fluka Chemical Co. Doubly distilled water was used in the experiments.

Sample preparation

The PVA/starch nanocomposite containing different percentages of GO was fabricated according to the solution casting technique. At first, 1 g of starch was dissolved in 20 mL of distilled water by heating at 95 °C for 30 min under vigorous stirring to induce starch gelatinization. Also, 1 g of PVA was dissolved in distilled water (30 mL) by heating at 90 °C for 30 min with continuous stirring until complete dissolution. These starch and PVA solutions were mixed together in the ratio 1:1, and then, glycerol (starch: glycerol ratio of 1:0.25) was added as plasticizer. The mixture was then continuously stirred (1000 rpm) for 30 min at room temperature. The suspension was further homogenized by ultrasonic treatment for 40 min. Finally, the suspensions were poured onto Petri plates to prepare the films. The bubbles formed during the preparation of the films were removed by using a vacuum oven. The blend films were dried at room temperature for 72 h.

The same procedure was applied for the preparation of the starch/PVA/GO nanocomposite except that different mass percentages of GO, i.e., 1, 2.5 and 5 mass%, were added to the starch and PVA solutions.

Characterizations

The thermal degradation of the samples was studied using a thermogravimetric analyzer (PL-STA 1500, UK) under nitrogen atmosphere at the heating rates of 5, 10, 15, and 20 °C min⁻¹ from ambient temperature to 600 °C. The morphology of the gold-coated films was investigated using a FESEM of Mira 3-XMU type with a Philips XL30-EDAX instrument (USA). The structure of the films was analyzed by a Philips advance XRD with Cu K-alpha radiation source ($\lambda = 0.1542$ nm) and a curved graphite crystal monochromator under 40 kV and 50 mA conditions.

DSC measurements were performed on a PerkinElmer DSC-7 differential scanning calorimeter in dry nitrogen (flow rate of 50 mL min⁻¹). The calorimeter was calibrated using high-purity indium. Dynamic DSC scans were conducted in the temperature range of 25–300 °C at four different heating rates of 5, 10, 15, and 20 °C min⁻¹.

FTIR spectra of the samples were recorded on a PerkinElmer FTIR Spectrum 100 spectrometer with universal ATR accessory between 4000 and 650 cm⁻¹ wavelength.

The viscoelastic properties were measured on a Triton 2000 DMTA (Triton Technology Co., England). DMTA tests were performed on the samples of 30 mm length, 10 mm width, and 0.5 mm thickness from – 40 to 180 °C at the fixed frequency of 1 Hz.

Theoretical background

The derivation of kinetic data in the study of polymer decomposition using TGA has received increasing attention in the last decade. The data obtained can be studied with a variety of techniques. These data depend on some factors including the flow rate of the gas and its nature, heating rate, sample mass, sample shape, and the mathematical treatment used to check the data. A reaction rate can be defined as the derivative of the conversion (α) with respect to time. The value of α can be determined in terms of mass loss from the TG curves as follows:

$$\alpha = \frac{m_0 - m}{m_0 - m_\infty} \quad (1)$$

where m is the measured mass of sample at temperature T , m_0 is the initial mass, and m_∞ is the mass at the end of the non-isothermal TGA experiment. The rate of conversion in a non-isothermal TGA experiment at a constant heating rate (β) can be expressed as follows:

$$\frac{d\alpha}{dt} = k(T)f(\alpha) \quad (2)$$

where $k(T)$ is the rate constant and $f(\alpha)$ is the conversion function. The rate constant k is described by the Arrhenius expression as:

$$k(T) = A \exp\left(-\frac{E_a}{RT}\right) \quad (3)$$

where E_a is the apparent activation energy, A is the pre-exponential factor, T is the absolute temperature, and R is the gas constant.

Substituting Eq. 3 into Eq. 2 gives:

$$\frac{d\alpha}{dt} = A \exp\left(-\frac{E_a}{RT}\right)f(\alpha) \quad (4)$$

If the sample temperature is changed with a controlled heating rate, $\beta = dT/dt$, the variation in the degree of conversion can be analyzed as a function of temperature which depends on the time of heating. Hence, the reaction rate may be shown as:

$$\frac{d\alpha}{dt} = \frac{d\alpha}{dT} \frac{dT}{dt} = \beta \frac{d\alpha}{dT} \quad (5)$$

where $\frac{d\alpha}{dT}$ is the non-isothermal reaction rate, $\frac{d\alpha}{dt}$ is the isothermal reaction rate, and $\frac{dT}{dt}$ is the heating rate (β). Substituting Eq. (4) into Eq. (5) gives:

$$\frac{d\alpha}{dT} = \frac{A}{\beta} \exp\left(-\frac{E_a}{RT}\right)f(\alpha) \quad (6)$$

Equations 4 and 6 are the fundamental expressions of analytical methods to calculate kinetic parameters based on TG data. Various models have been developed based on

these equations, and some of the most frequently used model-free methods in the study of polymers are listed in Table 1.

We used master plots to estimate a solid-state kinetic model that has the best match with the theoretical data [29–35]. By knowing the values of the activation energies and the kinetic model, the pre-exponential factor and the time to reach a definite conversion for the Kissinger equation can be calculated [36–39].

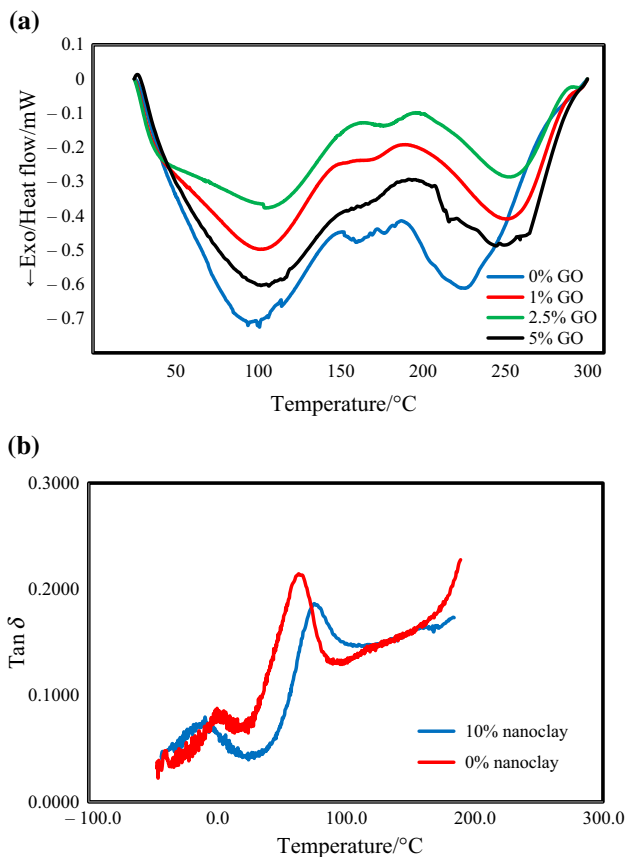
Results and discussion

DSC analysis

Figure 1a shows the DSC curves of starch/PVA film and its nanocomposites incorporated with different contents of GO. Table 2 demonstrates some important data obtained from DSC curves at the heating rate of $10 \text{ }^\circ\text{C min}^{-1}$. According to Fig. 1a, the T_g of the starch/PVA blend was $63 \text{ }^\circ\text{C}$, while it increased to 73 when 2.5 mass% of GO was added. The highest T_g was observed for the nanocomposite containing 2.5 mass% of GO. The enhanced T_g indicates new hydrogen interactions between the matrix and GO, since the mobility of polymer chains was restricted with the addition of GO. The DSC curves of the starch/PVA film exhibited an exothermic peak (typical of a semicrystalline polymeric system) at about $225 \text{ }^\circ\text{C}$, corresponding to the melting point of the formed crystalline regions when starch is retrograded. Increasing the GO content results in the increase in melting point, which also confirms that GO acts as a nucleating agent and prompts the crystallization of a matrix. In the other words, with increasing GO, the more physical entanglement of the polymer chains increases the synergistic interactions between PVA and starch, resulting in the increase of the T_m . As listed in Table 2, in the first peak, the PVA/starch/2.5% GO nanocomposite has a higher ΔH value than other nanocomposites (T_{peak1} up to $106 \text{ }^\circ\text{C}$). Because when GO is introduced into the blending system containing starch and PVA, the higher stability and intensity of hydrogen bonds newly formed between GO, starch, and PVA is strong enough to produce synergistic effect toward higher energy stability. Furthermore, DSC experiments at different concentrations of GO were performed in order to determine the optimum concentration. The highest reaction heat of 75.29 mW is related to the concentration of 2.5% GO (in the first peak). Also, the T_g values were determined by DMTA. Figure 1b shows the DMTA curves of starch/PVA film and its nanocomposites incorporated with 2.5% of GO. At fixed frequency, the value of $\tan \delta$ reaches maximum at glass transition temperature. The $\tan \delta$ curves give information about the damping and molecular mobility, which in turn is

Table 1 Solid-state kinetic model with corresponding symbols, differential conversion functions $f(\alpha)$ and integral conversion functions $g(\alpha)$

Kinetic model	Symbol	$g(\alpha)$	$f(\alpha)$
First order	F_1	$-\ln(1-\alpha)$	$1-\alpha$
Second order	F_2	$[(1-\alpha)-1]-1$	$(1-\alpha)^2$
Third order	F_3	$(1/2)[(1-\alpha)-2-1]$	$(1-\alpha)^3$
1. Diffusion	D_1	α^2	$1/(2\alpha)$
1. D diffusion	D_2	$(1-\alpha)\ln(1-\alpha)+\alpha$	$[-\ln(1-\alpha)]^{-1}$
2. D diffusion	D_3	$[1-(1-\alpha)1/3]^2$	$3/2[(1-\alpha)^{1/3}-1]$
Contracting area	R_2	$1-(1-\alpha)^{1/2}$	$2(1-\alpha)^{1/2}$
Contracting volume	R_3	$1-(1-\alpha)^{1/3}$	$3(1-\alpha)^{2/3}$
Two-dimensional nucleation	A_2	$[-\ln(1-\alpha)]^{1/2}$	$2(1-\alpha)[- \ln(1-\alpha)]^{1/2}$
Three-dimensional nucleation	A_3	$[-\ln(1-\alpha)]^{1/3}$	$3(1-\alpha)[- \ln(1-\alpha)]^{2/3}$
Four-dimensional nucleation	A_4	$4(1-\alpha)[- \ln(1-\alpha)]^3$	$4(1-\alpha)[- \ln(1-\alpha)]^{3/4}$

**Fig. 1** **a** DSC curves of the PVA/starch film and its nanocomposites containing different GO contents, **b** Curves of $\tan \delta$ of the PVA/starch film and its nanocomposite (2.5% GO)

connected to the impact strength of the sample. Comparing the $\tan \delta$ curves for both systems shows that incorporation of 2.5% GO results in the increase of the sample damping.

Table 2 DSC results of PVA/starch blend and its nanocomposite containing different contents of GO at the heating rate of $10^\circ\text{C min}^{-1}$ for **a** the first and **b** the second peaks

GO content/%	$T_p/^\circ\text{C}$	$T_m/^\circ\text{C}$	$\Delta H/\text{mW}$
(a)			
0	92	63	- 18.314
1	96	68	- 65.40
2.5	101	73	- 75.29
5	98	66	- 73.98
(b)			
0	221	207	- 66.05
1	248	220	- 91.84
2.5	251	225	- 67.27
5	242	213	- 115.71

Thermal stability of PVA/Starch/GO systems

TGA measurements can serve as a useful indicator for material flammability [40, 41]. The mass loss of a material due to the formation of volatile compounds under thermal degradation can be monitored using TGA measurements. Figure 2a shows the curves of mass loss against temperature at different heating rates for the PVA/starch/GO system. Accordingly, the TG curves were moved to higher temperatures by increasing the heating rate. Therefore, a shorter time is required for the samples to reach a given temperature at higher heating rates. The DTG curves for the PVA/starch/GO nanocomposite at the heating rate of $10^\circ\text{C min}^{-1}$ are shown in Fig. 2b. T_{initial} (at 5 mass% loss), T_{max} (at 95 mass% loss), and the residual mass at 600°C (W_{residual}) of the corresponding studied systems are listed in Table 3.

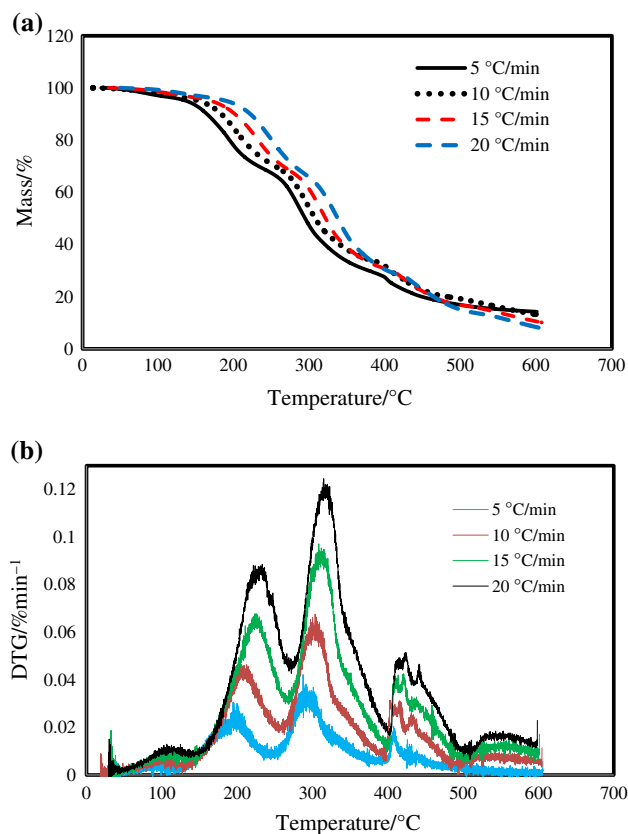


Fig. 2 **a** TG and **b** DTG curves of the PVA/starch/2.5% GO nanocomposite recorded at various heating rates of 5, 10, 15, and 20 °C min⁻¹ under nitrogen atmosphere

Table 3 Values of characteristic temperature (T_i , T_{max}) and W_{red} for degradation of PVA/starch blend and its nanocomposite at different heating rates

	$\beta/^\circ\text{C min}^{-1}$	$T_i/^\circ\text{C}$	$T_{max}/^\circ\text{C}$	$W_{red}/\%$
PVA/starch	5	173	410	4.12
	10	183	441	4.69
	15	187	448	4.80
	20	189	472	4.90
PVA/starch/GO (1%)	5	168	450	7.20
	10	175	470	7.68
	15	183	475	7.73
	20	186	491	7.85
PVA/starch/GO (2.5%)	5	165	471	14.15
	10	171	492	11.70
	15	177	496	11.09
	20	182	502	9.30
PVA/starch/GO (5%)	5	167	465	8.17
	10	173	480	8.43
	15	179	487	8.73
	20	184	495	8.82

According to the obtained results, the $T_{initial}$ and T_{max} values increase with increasing heating rates. But, $T_{initial}$ decreases by increasing the amount of GO. The lower $T_{initial}$ for the nanocomposite may be related to the role of GO which can hinder the participation of PVA and starch in the blend, and therefore, it can decrease the cross-linking of the PVA and starch. As a result, some unmixed PVA and starch may be present in the system. The values of T_{max} increased by increasing the amount of GO. The higher T_{max} for the nanocomposite is attributed to the enhancement of the interactions between the matrix and the GO, which limits the segmental movement of the polymer. Also, with the increase in GO, the thermal stability of the nanocomposites increased dramatically because of the increased mass residue after thermal decomposition. The GO acts as a mass transport barrier to the volatile products generated during thermal decomposition, leading to the retardance of the thermal degradation action. In addition, hydrogen bonding interactions between GO and PVA/starch matrix can decrease the quality of free -OH groups and stabilize the matrix. In the DTG curves of the PVA/starch (Fig. 2b), there are three distinct regions of mass loss. The first stage, which is below 200 °C (about 10 mass%), represents the volatilization of the easily degraded components such as glycerol and water. The second stage in the temperature range of 250–390 °C is related to the degradation of the PVA/starch blend. This stage is the most important stage in which polymers are degraded. In fact, the degradation process is initiated in the PVA amorphous regions. This stage of degradation can be attributed to the removal of hydroxyl groups in the PVA side chains which occurs simultaneously with the degradation of starch occurring in the range of 230–330 °C with a mass loss of 25%. In fact, in the second stage, we have a dehydroxylation process with the formation of carbon–carbon double bonds along the polymer backbone. The third stage is attributed to the scission of the residual main chains of PVA and starch occurring in the range 330–430 °C with a mass loss of about 75 mass%. Furthermore, the residue of the PVA/starch/GO nanocomposite is higher than that of the PVA/starch blend at 530 °C. The higher thermal degradation of the nanocomposite is attributed to the enhancement of the interactions between the matrix and the GO, which limit the segmental movement of the polymer. Figure 3 shows conversion curve versus temperature for different percentages of GO at the heating rate of 10 °C min⁻¹. Increasing the percentage of GO led to the completion of the degradation process at a higher temperature. As expected, with increasing the GO content, each conversion occurred at a higher temperature. Therefore, the GO-added PVA/starch blends have rather higher specific T values than the GO-unfilled PVA/starch, which might mean that the

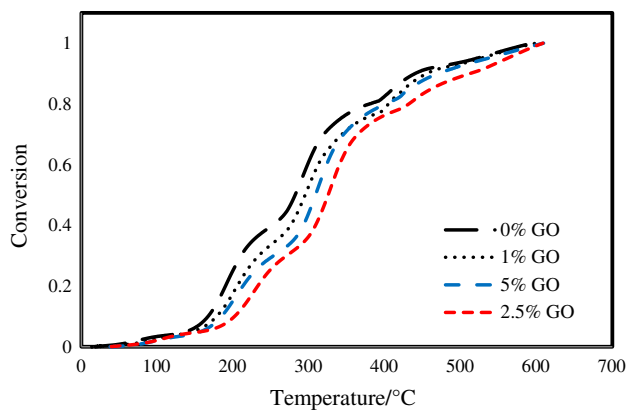


Fig. 3 Degree of conversion versus temperature for PVA/starch nanocomposites at various percentages of GO

addition of GO leads to the higher thermal stability of the PVA/starch.

Degradation kinetics

We used the non-isothermal TG data to determine the apparent activation energies of the PVA/starch/GO nanocomposite. The values of the E_a were calculated using Friedman [36], and KAS [37]. Figure 4 illustrates the relationship between the activation energy E_a and the degree of conversion for the PVA/starch film and its nanocomposites containing different GO contents. Figure 4a, b shows the presence of the nanomaterial in the PVA/starch blend results in the increase in the degradation activation energy. It is commonly known that the thermal degradation is initiated in weak link sites, and therefore, the activation energy for earlier stages is lower. According to Fig. 4a, the values of E_a up to $\alpha < 0.3$ are related to the first stage of the thermal degradation. The values of E_a in the ranges of $0.3 < \alpha < 0.6$ and $0.6 < \alpha < 0.85$ are related to the second and third stages, respectively. It can be observed that the mean values of E_a in the first, second and third stages for the PVA/starch blend are 86 ± 3 , 142 ± 2 and 145 ± 3 kJ mol^{-1} and for PVA/starch/2.5% GO nanocomposite are 108 ± 3 , 175 ± 4 and 176 ± 2 kJ mol^{-1} , respectively. As seen from the figure, at each step, the activation energy initially increases and then decreases. Clearly, the activation energy sometimes shows a fast drop. It is at the point of transition from one mass loss step to another. According to Fig. 4b, the value of E_a is calculated from the slope of a plot of $\ln(\beta/T_\alpha^2)$ against $1/T_\alpha$ at a fixed conversion. It can be observed that the mean values of E_a in the ranges of $0.3 < \alpha < 0.6$ and $0.6 < \alpha < 0.85$ for PVA/starch blend are 146 ± 2 and 148 ± 3 kJ mol^{-1} and for PVA/starch/2.5% GO nanocomposite are 176 ± 2 and 179 ± 3 kJ mol^{-1} , respectively. As a result, the mean values of E_a for the first,

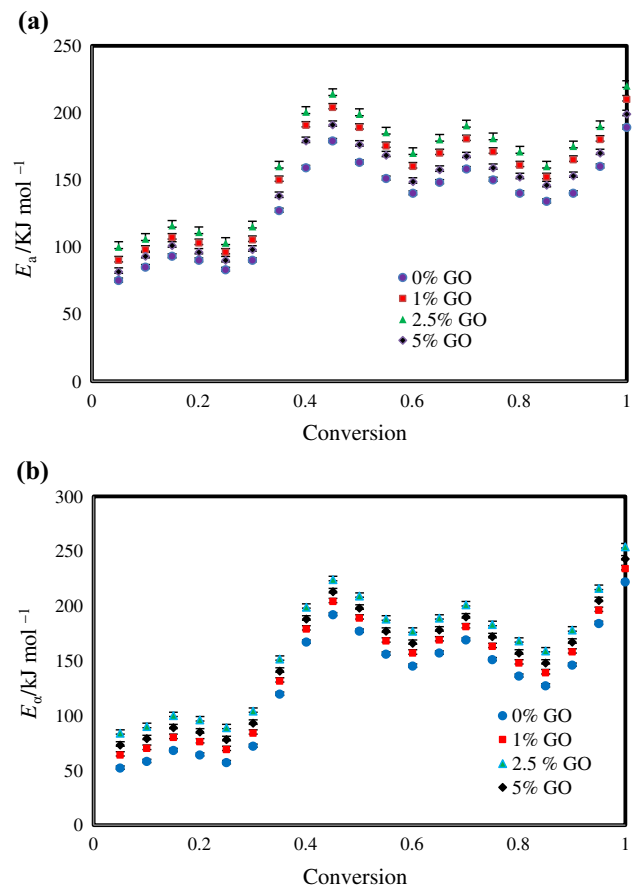


Fig. 4 Dependence of E_a on the extent of conversion for the PVA/starch film and its nanocomposites containing different GO contents using **a** the Friedman **b** KAS methods

second and third stages are determined by the two model-free isoconversional methods, which are in reliable agreement with each other. It is concluded that the E_a values are less for the first step and increase in the second and third steps in two methods. This indicates that the PVA/starch/GO nanocomposite is in need of lesser energy to remove the volatilization of the easily degraded components such as glycerol and water, whereas in the second and third steps it needs higher to remove the energy hydroxyl groups in the PVA side chains and starch and the bond scission and unzipping of carbon-carbon double bonds along the polymer backbone. However, the E_a values for the GO-unfilled PVA/starch are obviously lower than the GO-added samples (Fig. 4), plausibly indicating that the addition of GO may be helpful to improve the thermal stability of the PVA/starch blend.

Differential master plot analysis

The accuracy of the selected model was checked by producing master curves of $f(\alpha)$ versus α for different mechanisms. Figure 5 shows the theoretical master plots with the

experimental master curve for the degradation of the PVA/starch/GO nanocomposite at the heating rate of $10\text{ }^\circ\text{C min}^{-1}$. The comparison of the experimental master plots with the theoretical ones indicates that the kinetic functions of the thermal degradation for the PVA/starch blend and the PVA/starch/GO nanocomposite can be most probably described by A_2 , $[-\ln(1-\alpha)]^{1/2}$, and A_3 , $[-\ln(1-\alpha)]^{1/3}$ models, respectively. The physical description of the A_2 and A_3 mechanisms is nucleation and growth.

Combined differential and integral master plot analysis

In order to further check the accuracy of the obtained degradation mechanism, the combined differential and integral master plots were also analyzed [42]. According to Fig. 6, at the heating rate of $10\text{ }^\circ\text{C min}^{-1}$, the experimental data of the PVA/starch/GO nanocomposite fit with the A_3 model. It should be noted that the model for the thermal degradation of the nanocomposite at other heating rates (5, 15 and $20\text{ }^\circ\text{C min}^{-1}$) was also found to be A_3 (data not shown). These results confirm our assumption that the thermal degradation of the PVA/starch/GO nanocomposite behaves as a three-step solid-state reaction.

Accordingly, the average value of A was determined to be 5.29×10^{16} and $8.44 \times 10^{13}\text{ min}^{-1}$ for the PVA/starch blend and nanocomposite, respectively. Therefore, the rate of the solid-state degradation process can be modeled for the nanocomposite and PVA/starch blend, respectively, as:

$$\frac{d\alpha}{dt} = 2 \times 8.44 \times 10^{13} \exp\left(\frac{-175000}{RT}\right) (1-\alpha) [-\ln(1-\alpha)]^{\frac{1}{2}} \tag{7}$$

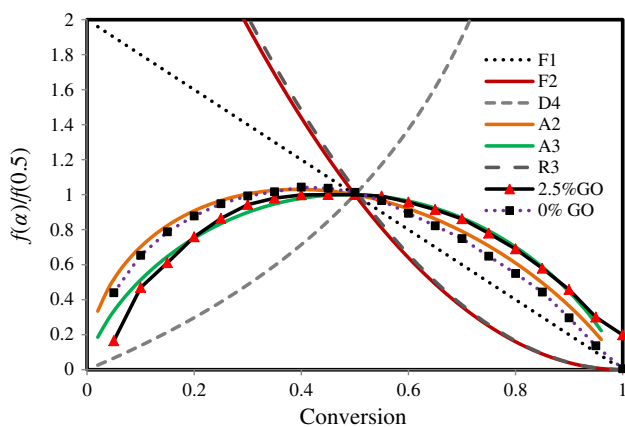


Fig. 5 Comparison of master curve plots for degradation of the PVA/starch blend and PVA/starch/2.5% GO nanocomposite at the heating rate of $10\text{ }^\circ\text{C min}^{-1}$

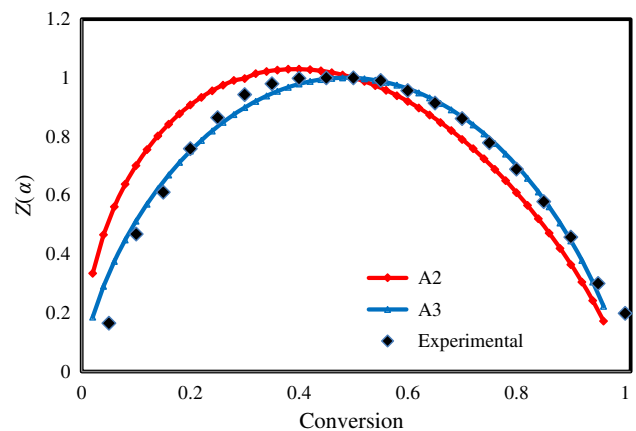


Fig. 6 The comparison of best-fitted experimental with theoretical master curve for PVA/starch/GO nanocomposite in combined form indicating $Z(\alpha)$ versus conversion

$$\frac{d\alpha}{dt} = 3 \times 5.29 \times 10^{16} \exp\left(\frac{-146000}{RT}\right) (1-\alpha) [-\ln(1-\alpha)]^{\frac{1}{3}} \tag{8}$$

It is obvious that the thermal degradation rate of the nanocomposite is lower than that of the PVA/starch blend, while the degradation time of the nanocomposite is higher than that of the PVA/starch blend. The rate constant was also derived from the Arrhenius equation as a function of temperature listed in Table 4. According to Table 4, a k value of the nanocomposite was lower than that of the PVA/starch blend.

The obtained equations of degradation time can be modeled for the nanocomposite and PVA/starch blend, respectively, as:

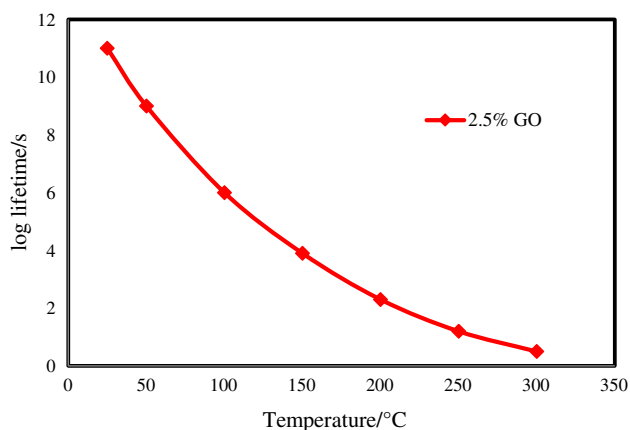
$$t_\alpha = \frac{[-\ln(1-\alpha)]^{\frac{1}{2}}}{8.44 \times 10^{13} \exp\left(\frac{-175000}{RT}\right)} \tag{9}$$

$$t_\alpha = \frac{[-\ln(1-\alpha)]^{\frac{1}{3}}}{5.29 \times 10^{16} \exp\left(\frac{-146000}{RT}\right)} \tag{10}$$

The major applications of these equations are to predict the optimum processing temperature regions, the maximum usable temperature and estimated lifetime of the PVA/starch/GO nanocomposite. The lifetime t_f is commonly described to be when the degree of decomposition reaches 5% [33]. It should be noted that the lifetime of the specimen is in a direct relation with its performance and thermal durability. For definition of lifetime of the PVA/starch/GO nanocomposite, $\alpha = 0.05$ must be appropriately substituted in Eq. (9). Figure 7 shows a logarithmic curve of lifetime versus temperature for the PVA/starch/GO nanocomposite. Based on the calculation shown above, the lifetime of the PVA/starch/GO nanocomposite at 25, 100 and $150\text{ }^\circ\text{C}$ are computed to be 3.61×10^3 , 0.02 and 0.003 years,

Table 4 Values of activation energy, degradation rate, pre-exponential factor, differential and integral kinetic functions of PVA/starch blend, and its nanocomposite (2.5% GO)

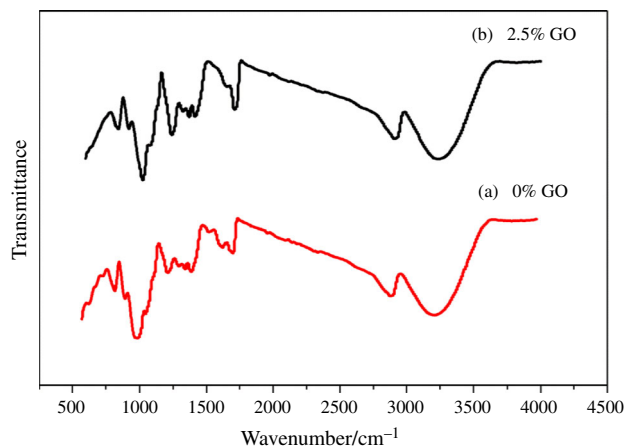
Sample	$E_a/\text{kJ mol}^{-1}$ (KAS)	A	k/min^{-1}	$f(\alpha)$	$g(\alpha)$
PVA/starch	146	5.29×10^{16}	2.65	$2(1 - \alpha)[- \ln(1 - \alpha)]^{1/2}$	$[- \ln(1 - \alpha)]^{1/2}$
PVA/starch/GO (2.5%)	175	8.44×10^{13}	0.79	$3(1 - \alpha)[- \ln(1 - \alpha)]^{2/3}$	$[- \ln(1 - \alpha)]^{1/3}$

**Fig. 7** Logarithm of lifetime as a function of temperature for the PVA/Starch/GO nanocomposite

respectively. The lifetime values show that the addition of GO can be helpful to improve the thermal stability of the PVA/starch blend.

Investigation on the interactions in the PVA/starch system

The hydrogen bonding plays an important role in the formation of interactions between starch, PVA and GO. These interactions can be identified by FTIR spectra. The changes in peak bandwidth, strength, and frequency provide valuable information to interpret the formation of intermolecular hydrogen bonding in the samples. According to Fig. 8a, for the polyvinyl alcohol and starch system, the strong and broad absorption peak at 3237 cm^{-1} is assigned to the stretching vibration of the OH group and the band at 2931 cm^{-1} is due to the stretching vibrations of the CH and CH_2 groups. The broad peak at 1729 cm^{-1} is assigned to the C=O stretching vibration mode, which is probably a coalescence peak caused by the ester bond and carboxyl C=O groups in the PVA, because PVA is obtained from the hydrolysis of polyvinyl acetate, and therefore, it is possible that not all polyvinyl acetate is hydrolyzed. The bands attributed to the CH and CH_2 deformation vibrations appear between 1300 and 1500 cm^{-1} . The bands located at 1415 and 846 cm^{-1} are assigned to the vibrations associated with the CH_2 group. The bands at 1000 – 1300 cm^{-1}

**Fig. 8** FTIR spectra for the PVA/starch film and its nanocomposite containing 2.5 mass% of GO

are attributed to the stretching vibrations of the C–O in the C–O–H and C–O–C groups. The effect of nanomaterial on the FTIR spectra of the PVA/starch blends is shown in Fig. 8b. In the optimum nanocomposite, the above-mentioned peaks are detectable with slight shifts, which are probably due to the presence of GO and the interactions between the nanomaterial and the polymer matrix. Therefore, by adding nanomaterial, the –OH stretching peak and C–O–H stretching peak shift to a lower wavenumber, indicating the presence of strong molecular interactions including the H-bonding between OH groups of PVA/starch matrix and the remaining oxygenated groups present on the GO surface.

XRD analysis

The influence of GO nanomaterial on the crystalline structure of PVA/starch in the nanocomposites prepared via solution casting was also investigated by means of XRD.

Figure 9 shows the X-ray diffraction patterns of neat PVA and starch, PVA/starch film and its nanocomposite containing 2.5 mass% GO. PVA is a semicrystalline polymer in which high physical interactions present between the polymer chains, due to hydrogen bonding between the hydroxyl groups exist. PVA has a diffraction peak at $2\theta = 19.4^\circ$ and is characteristic for an

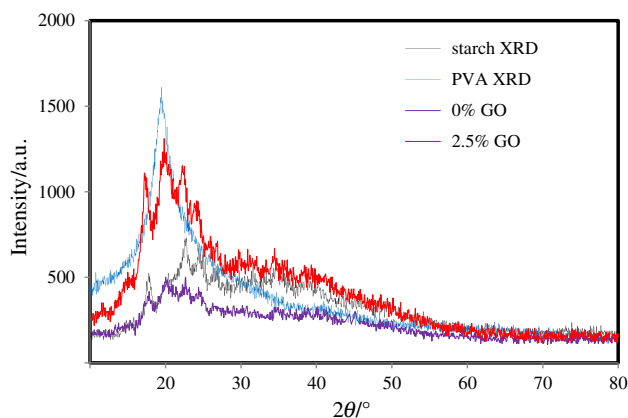


Fig. 9 XRD patterns of the pure PVA, pure starch, PVA/starch films and PVA/starch nanocomposite films containing 2.5 mass% of GO prepared via solution casting method

orthorhombic lattice. Starch has a number of well-resolved peaks overlapping an amorphous hump. The peaks of neat starch film appear at $2\theta = 17.84, 20.100980, 22.664480, 24.576620, 26.576730, 34.663520, 38.552520$. The peaks of the starch/PVA film appear at $2\theta = 13.8417, 18.0449, 20.5487$. These peaks show that the crystallinity changed after mixing. The crystallinity of PVA decreased, indicating that the crystal structure was changed after being cross-linked with starch, whose vice-bond was broken and the crystal was destroyed. When forming the film, the interface bonding formed between starch and PVA may result in a decrease in the number of hydrogen bonds. Therefore, the decreased PVA crystallinity indicates the strong interaction present between the starch and PVA polymer chains after cross-linking. The nanocomposite shows some peaks at $2\theta = 17.7371, 20.0988, 22.5405, 24.3871$. It is obvious that the nanocomposites displayed similar diffraction pattern at the same 2θ positions as the starch/PVA film. Consequently, the presence of GO displayed no effect on the crystal structures of the PVA/starch matrix in the nanocomposites. Moreover, in the nanocomposites, the peak intensity on the crystal structures of the PVA/starch matrix increases, which can be attributed to the incorporation of GO nanomaterial within the starch/PVA film.

Scanning electron microscopy

The morphology of the studied samples was studied using FESEM micrographs (Fig. 10). According to Fig. 10a, a homogeneous morphology can be seen for the PVA/starch blend, which proves the miscibility of PVA in starch. In the PVA/starch/GO nanocomposites (Fig. 10b), the layers in the form of bright lines are uniformly dispersed throughout the matrix. Possibly, the hydroxyl groups of PVA and starch chains interacts well with the oxygen-containing groups present in the layers of GO. Therefore, the affinity

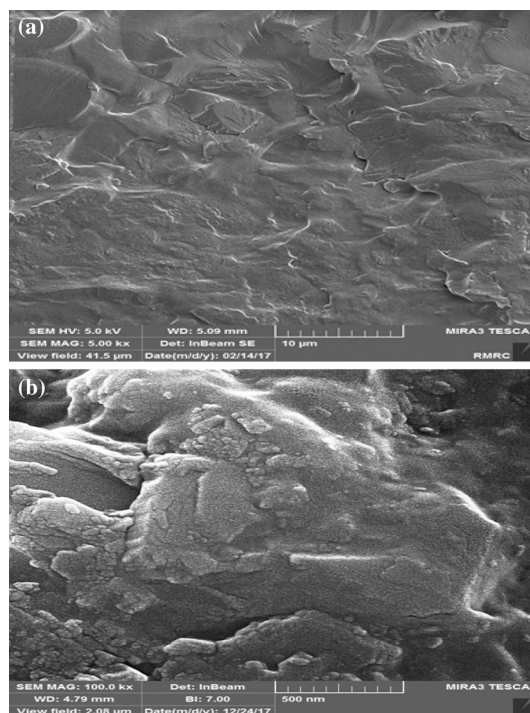


Fig. 10 FESEM images of **a** PVA/starch film and **b** PVA/starch film containing 2.5 mass% of GO

among GO and PVA/starch chains leads to the exfoliation of GO layers in the PVA matrix. However, a relatively homogeneous morphology was observed between the PVA/starch matrix and GO.

Conclusions

Study on the thermal degradation behavior of the PVA/starch/GO nanocomposite showed a three-stage mass loss. The mater plots were constructed to investigate the non-isothermal degradation kinetics. For this aim, the experimental data, obtained under a linear heating rate, were used to determine the activation energies by means of the model-free isoconversional approaches. The results indicated that the values of activation energies varied significantly with the extent of conversion. By the comparison between the theoretical and experimental master curves, the thermal degradation mechanisms of the starch/PVA blend and starch/PVA/GO nanocomposite were evaluated to be A_2 and A_3 , respectively. Accordingly, the average values of pre-exponential factors were determined to be 5.29×10^{16} and $8.44 \times 10^{13} \text{ min}^{-1}$ for the PVA/starch film and nanocomposite, respectively. The kinetic analysis showed that the degradation rate of the PVA/starch/GO nanocomposite was lower than that of the PVA/starch film. However, the degradation time of the nanocomposite was higher than that of the PVA/starch film. Therefore, it can be

deduced that the PVA/starch/GO nanocomposite can be used in some applications where low to medium temperatures are required for a very long time. FESEM photographs revealed that the GO dispersed well in the PVA/starch matrix. This dispersion is useful to improve the mechanical properties of the film. XRD and FTIR analyses further confirmed the distribution of GO in the PVA/starch matrix. Based on the DSC, when the GO content increased, the peaks shifted to higher temperatures. On the other hand, the thermal stability can be improved by increasing the GO content and the crystallinity change. Furthermore, the optimum content of the GO was determined to be 2.5 mass% based on the T_g and ΔH .

Acknowledgements The financial support from University of Mazandaran is gratefully acknowledged.

References

- Olewnik E, Garman K, Czerwiński W. Thermal properties of new composites based on nanoclay polyethylene and polypropylene. *J Therm Anal Calorim.* 2010;101:323–9.
- Avérous L, Halley P-J. Biocomposites based on plasticized starch. *Biofuels Bioprod Biorefin.* 2009;3:329–43.
- Zia F, Zia K-M, Zuber M, Kamal S, Aslam N. Starch based polyurethanes: a critical review updating recent literature. *Carbohydr Polym.* 2015;134:784–98.
- Stojanović Ž, Katsikas L, Popović I, Jovanović S, Jeremić K. Thermal stability of starch benzoate. *Polym Degrad Stab.* 2005;87:177–82.
- Zhai M, Yoshii F, Kume T, Hashim K. Syntheses of PVA/starch grafted hydrogels by irradiation. *Carbohydr Polym.* 2002;50:295–303.
- Cano A, Fortunati E, Cháfer M, Kenny JM, Chiralt A, González-Martínez C. Properties and ageing behaviour of pea starch films as affected by blend with poly (vinyl alcohol). *Food Hydrocoll.* 2015;48:84–93.
- Jiménez A, Fabra MJ, Talens P, Chiralt A. Edible and biodegradable starch films: a review. *Food Bioprocess Technol.* 2012;5:2058–76.
- Taghizadeh M-T, Abdollahi R. A kinetics study on the thermal degradation of starch/poly (vinyl alcohol) blend. *Chem Mater Eng.* 2015;3:73–8.
- Xie F, Pollet E, Halley P-J, Avérous L. Starch-based nano-biocomposites. *Prog Polym Sci.* 2013;38:1590–628.
- Adebowale K-O, Afolabi T-A, Olu-Owolabi B-I. Functional, physicochemical and retrogradation properties of sword bean (*Canavalia gladiata*) acetylated and oxidized starches. *Carbohydr Polym.* 2006;65:93–101.
- Warren F-J, Gidley M-J, Flanagan B-M. Infrared spectroscopy as a tool to characterise starch ordered structure a joint FTIR-ATR, NMR, XRD and DSC study. *Carbohydr Polym.* 2016;139:35–42.
- Cano A, Jiménez A, Cháfer M, González C, Chiralt A. Effect of amylose: amylopectin ratio and rice bran addition on starch films properties. *Carbohydr Polym.* 2014;111:543–55.
- Forssell P-M, Hulleman S-H, Myllärinen P-J, Moates G-K, Parker R. Ageing of rubbery thermoplastic barley and oat starches. *Carbohydr Polym.* 1999;39:43–51.
- Sukhija S, Singh S, Riar C-S. Physicochemical, crystalline, morphological, pasting and thermal properties of modified lotus rhizome (*Nelumbo nucifera*) starch. *Food Hydrocoll.* 2016;60:50–8.
- Priya B, Gupta V-K, Pathania D, Singha A-S. Synthesis, characterization and antibacterial activity of biodegradable starch/PVA composite films reinforced with cellulosic fibre. *Carbohydr Polym.* 2014;109:171–9.
- Aydın A-A, Ilberg V. Effect of different polyol-based plasticizers on thermal properties of polyvinyl alcohol: starch blends. *Carbohydr Polym.* 2016;136:441–8.
- Cano A-I, Cháfer M, Chiralt A, González-Martínez C. Physical and microstructural properties of biodegradable films based on pea starch and PVA. *J Food Eng.* 2015;167:59–64.
- Ortega-Toro R, Jiménez A, Talens P, Chiralt A. Properties of starch-hydroxypropyl methylcellulose based films obtained by compression molding. *Carbohydr Polym.* 2014;109:155–65.
- Nistor M-T, Vasile C. Influence of the nanoparticle type on the thermal decomposition of the green starch/poly (vinyl alcohol)/montmorillonite nanocomposites. *J Therm Anal Calorim.* 2013;111:1903–19.
- Majdzadeh-Ardakani K, Nazari B. Improving the mechanical properties of thermoplastic starch/poly (vinyl alcohol)/clay nanocomposites. *Compos Sci Technol.* 2010;70:1557–63.
- Noshirvani N, Hong W, Ghanbarzadeh B, Fasihi H, Montazami R. Study of cellulose nanocrystal doped starch-polyvinyl alcohol bionanocomposite films. *Int J Biol Macromol.* 2017;107:2065–74.
- Abd-Elrahman M-I. Enhancement of thermal stability and degradation kinetics study of poly (vinyl alcohol)/zinc oxide nanoparticles composite. *J Thermoplast Compos Mater.* 2014;27:160–6.
- Usman A, Hussain Z, Riaz A, Khan A-N. Enhanced mechanical, thermal and antimicrobial properties of poly (vinyl alcohol)/graphene oxide/starch/silver nanocomposites films. *Carbohydr Polym.* 2016;153:592–9.
- Ferreira W-H, Andrade C-T. Characterization of glycerol-plasticized starch and graphene oxide extruded hybrids. *Ind Crops Prod.* 2015;77(23):684–90.
- Li R, Liu C, Ma J. Studies on the properties of graphene oxide-reinforced starch biocomposites. *Carbohydr Polym.* 2011;84:631–7.
- Peregrino P-P, Sales M-J-A, da Silva M-F-P, Soler M-A-G, da Silva L-F-L, Moreira S-G-C, Paterno L-G. Thermal and electrical properties of starch-graphene oxide nanocomposites improved by photochemical treatment. *Carbohydr Polym.* 2014;106:305–11.
- Beeran Y, Bobnar V, Gorgieva S, Grohens Y, Finsgar M, Thomas S, Kokol V. Mechanically strong, flexible and thermally stable graphene oxide/nanocellulosic films with enhanced dielectric properties. *RSC Adv.* 2016;6:49138–49.
- Sadhu SD, Soni A, Garg M. Thermal studies of the starch and polyvinyl alcohol based film and its nano composites. *J Nanomedic Nanotechnol S.* 2015;7:2.
- Vyazovkin S, Chrissafis K, Di Lorenzo M-L, Koga N, Pijolat M, Roduit B, Suñol J-J. ICTAC kinetics committee recommendations for collecting experimental thermal analysis data for kinetic computations. *Thermochim Acta.* 2014;590:1–23.
- Slopiecka K, Bartocci P, Fantozzi F. Thermogravimetric analysis and kinetic study of poplar wood pyrolysis. *Appl Energy.* 2012;97:491–7.
- Vyazovkin S, Dollimore D. Linear and nonlinear procedures in isoconversional computations of the activation energy of non-isothermal reactions in solids. *J Chem Inf Model.* 1996;36:42–5.
- Senum G-I, Yang R-T. Rational approximations of the integral of the Arrhenius function. *J Therm Anal.* 1977;11:445–7.
- Perez-Maqueda L-A, Criado J-M. Accuracy of Senum and Yang's approximations to the Arrhenius integral. *J Therm Anal Calorim.* 2000;60:909–15.

34. Criado J-M, Málek J, Ortega A. Applicability of the master plots in kinetic analysis of non-isothermal data. *Thermochim Acta*. 1989;147:377–85.
35. Paterson W-L. Computation of the exponential trap population integral of glow curve theory. *J Comput Phys*. 1971;7:187–90.
36. Friedman H. Kinetics and gaseous products of thermal decomposition of polymers. *J Macromol Sci*. 1967;79:37–41.
37. Kissinger H-E. Reaction kinetics in differential thermal analysis. *Anal Chem*. 1957;29:1702–6.
38. Malek J. The kinetic analysis of non-isothermal data. *Thermochim Acta*. 1992;200:257–69.
39. Sestak J, Malek J. Diagnostic limits of phenomenological models of heterogeneous reactions and thermal analysis kinetics. *Solid State Ion*. 1993;63:245–54.
40. Zhou L, Luo T, Huang Q. *Energy Convers Manage*. 2009;50:705.
41. Zhaosheng Y, Xiaoqian M, Ao L. *Energy Convers Manage*. 2009;50:561.
42. Gotor F-J, Criado J-M, Malek J, Koga N. Kinetic analysis of solid-state reactions: the universality of master plots for analyzing isothermal and nonisothermal experiments. *J Phys Chem A*. 2000;104:10777–82.